

# Role of the Azadithiolate Cofactor in Models for the [FeFe]-Hydrogenase: Novel Structures and Catalytic Implications

*Matthew T. Olsen, Thomas B. Rauchfuss, Scott R. Wilson*

*Department of Chemistry*

*University of Illinois at Urbana-Champaign*

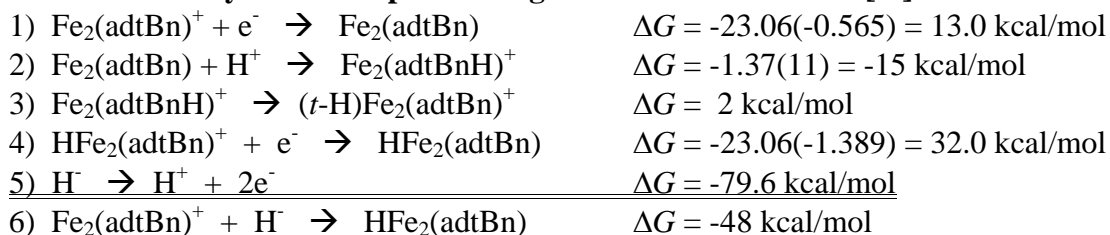
*Urbana, IL 61801*

- 1. Thermodynamic Calculations**
- 2.  $pK_a$  Measurements**
- 3. Dications**
- 4. Decomposition of  $[2']^+$  and  $[2']^{2+}$  with  $O_2$**
- 5. Kinetic Analysis of the Reaction of  $[H2']^+$  with TEMPO**
- 6. Electrochemistry**

- 1. Thermodynamic Calculations**

**General Comments on Thermodynamics and Solvent Effects.** Throughout the literature, MeCN is the solvent of choice for the thermodynamic analysis of metal hydrogen chemistry.<sup>1</sup> This is primarily a consequence of limited availability of the thermochemical parameters for the heterolysis of H<sub>2</sub>, which is available in MeCN (as well as H<sub>2</sub>O and DMSO).<sup>2</sup> Thus, electrochemical measurements were performed in MeCN, and pK<sub>a</sub> values were estimated based on known values in MeCN. However, these solvents are incompatible with H<sub>ox</sub> models because of degradation reactions that occur in the presence of such coordinating solvents. Thus, all other direct studies of H<sub>ox</sub> models were enabled by the use of the non-coordinating solvent CH<sub>2</sub>Cl<sub>2</sub>.

**A. Estimation of Hydride Acceptor Strengths for the Monocation [2']<sup>+</sup>:**



*Comments:*

eq 1): For [2']<sup>0/+</sup> couple, E<sub>1/2</sub> = -0.565 V. *Conditions:* 1mM [2'], MeCN soln., 100 mM [Bu<sub>4</sub>N]PF<sub>6</sub>, 20 °C.

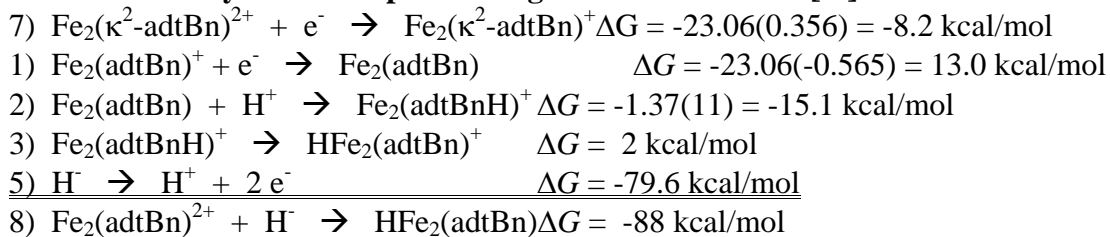
eq 2): The pK<sub>a</sub><sup>MeCN</sup>(2'H<sup>+</sup>) was estimated at 11.15 based on the pK<sub>a</sub><sup>MeCN</sup> of [Fe<sub>2</sub>[(SCH<sub>2</sub>)<sub>2</sub>NHMe](CO)<sub>6</sub>]<sup>+</sup> and [Fe<sub>2</sub>[(SCH<sub>2</sub>)<sub>2</sub>NH<sub>2</sub>](CO)<sub>4</sub>(PMe<sub>3</sub>)<sub>2</sub>]<sup>+</sup> of 8.14 and 10.15, respectively.<sup>3</sup> This estimate assumes one pK<sub>a</sub><sup>MeCN</sup> unit per tertiary phosphine.

eq 3): The terminal hydride tautomers of [2'H]<sup>+</sup> and [2H]<sup>+</sup>, respectively [H2']<sup>+</sup> and [H2]<sup>+</sup>, are not detected in the -80 °C <sup>1</sup>H and <sup>31</sup>P NMR spectra of the ammonium compounds, indicating that K > 30 (conservative detection limit for <sup>1</sup>H NMR spectra).

eq 4): The redox couples for the terminal hydrides [t-H2']<sup>0/+</sup> (which are not observable), are estimated from E<sub>1/2</sub> for [μ-H2']<sup>0/+</sup> and [μ-H2]<sup>0/+</sup>, which in MeCN solution are -1.50. The difference between E<sub>1/2</sub><sup>[t-H2']<sup>0/+</sup></sup> and E<sub>1/2</sub><sup>[μ-H2]<sup>0/+</sup></sup> is provided by the difference between E<sub>1/2</sub> for [t-HFe<sub>2</sub>(pdt)(CO)<sub>2</sub>(dppv)<sub>2</sub>]<sup>+0</sup> and E<sub>1/2</sub> for [μ-HFe<sub>2</sub>(pdt)(CO)<sub>2</sub>(dppv)<sub>2</sub>]<sup>+0</sup>, which is 0.200 V.<sup>4</sup> The potential of E<sub>1/2</sub> for the [2(μ-H)]<sup>+0</sup> couple is -1.589 V. We estimate therefore that of the terminal hydride is 0.2 V milder, i.e. -1.389 V.

eq 5): This value has been reported for MeCN solution.<sup>2</sup>

**B. Estimation of Hydride Acceptor Strengths for the dication [2']<sup>2+</sup>:**

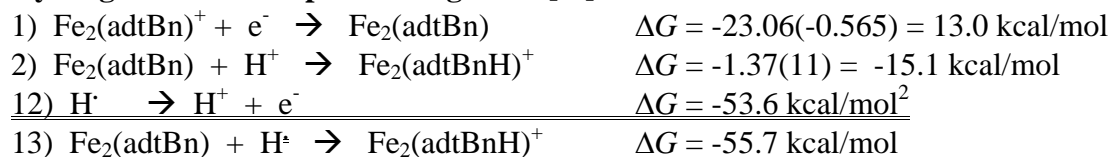


*Notes:*

eq 1,2,3,4,5): see section A above.

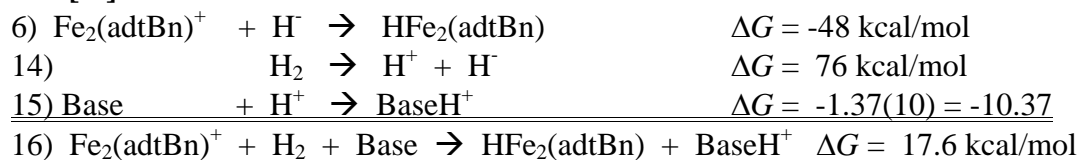
eq 7): The  $1^{+/2+}$  redox potential is used as an approximation of the  $2^{+/2+}$  potential *in the absence of amine binding*. Using  $E_{1/2}(1^{+/2+})$  allows us to approximate the hydride acceptor strength at a terminal site (which would otherwise be occupied by amine in the  $\kappa^3$ -adt complex). Because the  $1^{+/2+}$  couple is complicated (see Electrochemistry section below) by MeCN, the values in  $\text{CH}_2\text{Cl}_2$  were used as approximations.

### C. Hydrogen Atom Acceptor Strength for $[2']^+$ :

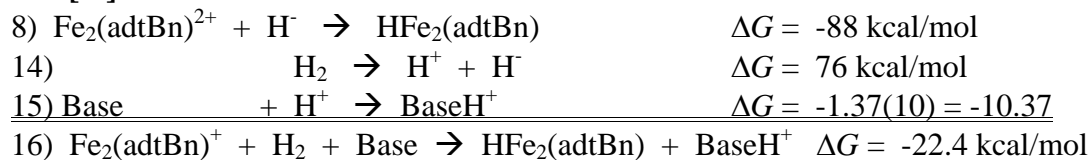


### D. Dihydrogen Heterolysis

For  $[2']^+$ :

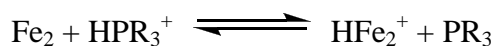


For  $[2']^{2+}$ :



## 2. $\text{pK}_a$ Measurements for **2** and **2'**

The  $\text{pK}_a$  values of **2** and **2'** were measured by titration against the phosphonium acid  $[\text{HPMe}_2\text{Ph}]\text{BF}_4$  ( $\text{pK}_a^{\text{CD}_2\text{Cl}_2} = 5.7$ ). Concentrations measured by the absorbances of non-overlapping peaks in the IR spectrum for **2** ( $1870\text{ cm}^{-1}$ ),  $[\text{H}_2]\text{BF}_4$  ( $1975\text{ cm}^{-1}$ ), **2'** ( $1944\text{ cm}^{-1}$ ), and  $[\text{H}_2']\text{BF}_4$  ( $1920\text{ cm}^{-1}$ ).



$$K_{eq} = ([\text{HFe}_2^+][\text{PR}_3])/([\text{Fe}_2][\text{HPR}_3^+])$$

$$[\text{HFe}_2^+] = [\text{PR}_3]$$

$$K_{eq} = [\text{HFe}_2^+]^2/([\text{Fe}_2][\text{HPR}_3^+])$$

$$[\text{HFe}_2^+]^2/[\text{Fe}_2] = K_{eq}[\text{HPR}_3^+]$$

For 2:

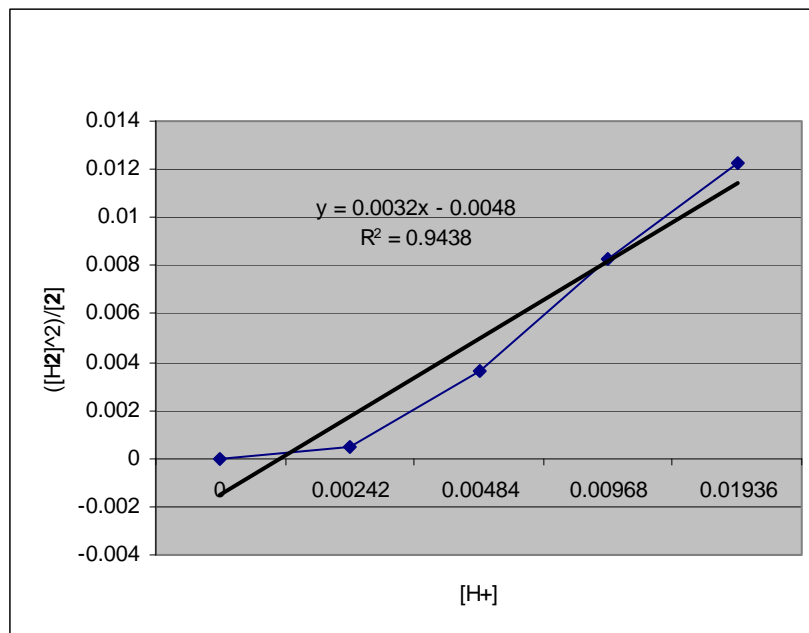


**Figure S1:** Plot of  $[H_2]^2/[2]$  vs  $[H^+]$ .

$$\begin{aligned} pK^{CD_2Cl_2} &= pK_{a,[HPMe_2Ph]BF_4} - [-\log(K_{eq})] \\ &= 5.7 + \log(0.0032) = 3.2 \end{aligned}$$

For 2':

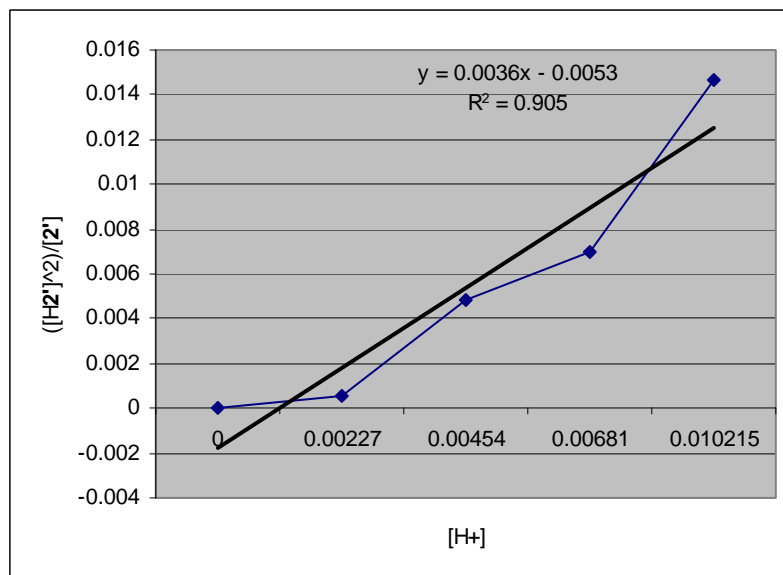


**Figure S2:** Plot of  $[H_2']^2/[2']$  vs  $[H^+]$ .

$$pK^{CD_2Cl_2} = pK_{a,[HPMe_2Ph]BF_4} - [-\log(K_{eq})]$$

$$= 5.7 + \log(0.0036) = 3.3$$

### 3. Dications $[2'](\text{BAr}^{\text{F}}_{24})_2$ and $[2'](\text{BF}_4)_2$

De Gioia and coworkers<sup>5</sup> have proposed that the structure of the ‘fully oxidized’ differrous ( $32e^-$ ) model compound  $[\text{Fe}_2(\text{S}_2\text{C}_3\text{H}_6)(\text{CN})_2(\text{CO})(\text{L}/\text{X})]^{0/-1}$  depends on the ligand set. When an X-type ligand (anionic, often a  $\pi$ -donor) is present, the model is isostructural with  $\text{H}_{\text{ox}}$  models, featuring a  $\mu$ -CO ligand and a vacant site on a single Fe. When an L-type ligand (neutral, moderate or weak donor) is present, the Fe-Fe distance is lengthened from  $\sim 2.5$  to  $\sim 2.8$  Å and an agostic interaction is observed between the central methylene of the propanedithiolate ligand, and a single Fe. Although these models lack the biorelevant azadithiolate cofactor, these structural trends may provide useful lessons with other model compounds.

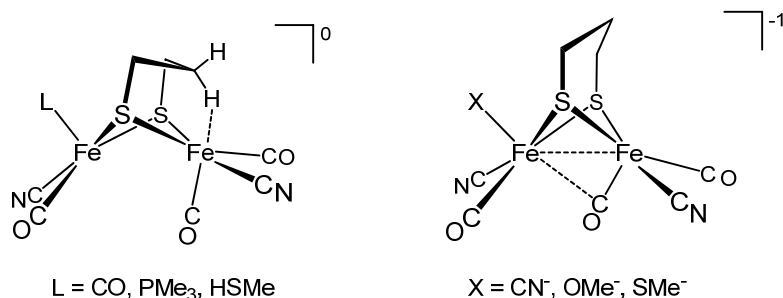


**Figure S3:** Structures of ‘naked’ ( $32e^-$ ) differrous dimers as computationally determined by De Gioia and coworkers.

Given the tendency of agostic coordination modes in unsaturated differrous species, it may be reasonable to assume that replacement of the central methylene with  $\text{NCH}_2\text{C}_6\text{H}_5$  would result in binding of the amine. We were unable to confirm the structure of the naked dication  $[2']^{2+}$ , although the adduct  $[2'(\text{NCMe})](\text{BF}_4)_2$  displays this bonding mode.

The  $^{31}\text{P}$  NMR spectrum of  $[2'](\text{BF}_4)_2$  indicates that it is *unsymmetrical* and the  $\text{PMe}_3$  resonance is  $\sim 20$  upfield of the corresponding resonance in  $[2'](\text{BAr}^{\text{F}}_{24})_2$ . The IR spectrum displays all terminal carbonyl bands but the relative intensities of the peaks are different when compared to  $[2'](\text{BAr}^{\text{F}}_{24})_2$ . These differences suggest that  $\text{BF}_4^-$  binding may be relevant to the dicatonic species  $[2']^{2+}$ .

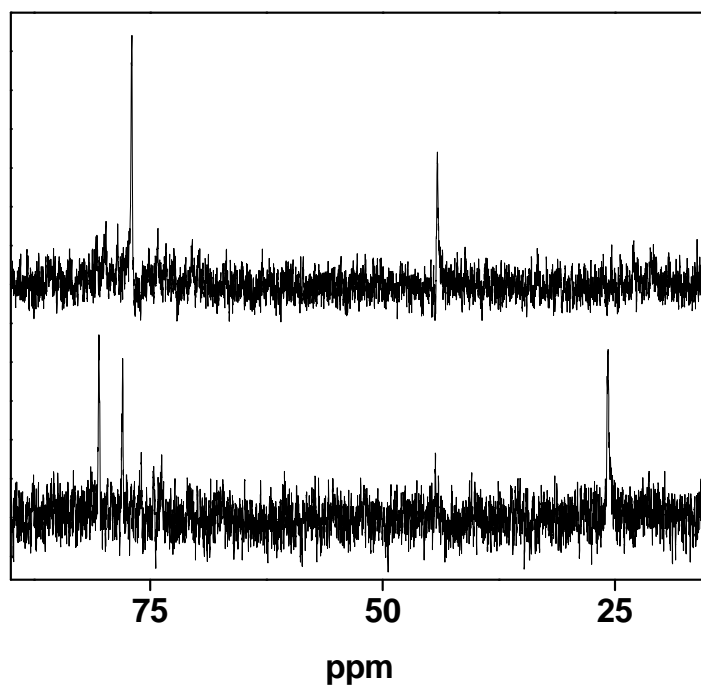


**Figure S4:** 202 MHz  $^{31}\text{P}$  NMR spectra ( $\text{CD}_2\text{Cl}_2$ ) at  $-70\text{ }^\circ\text{C}$  for  $[\mathbf{2}'](\text{BAr}^{\text{F}}_{24})_2$  (top) and  $[\mathbf{2}'](\text{BF}_4)_2$  (bottom). The low resolution is due to limited solubility from low temperature sample preparation.

Upon warming,  $^{31}\text{P}$  NMR spectroscopy indicated that  $[\mathbf{2}'](\text{BAr}^{\text{F}}_{24})_2$  converted to a complex mixture of unknown products.

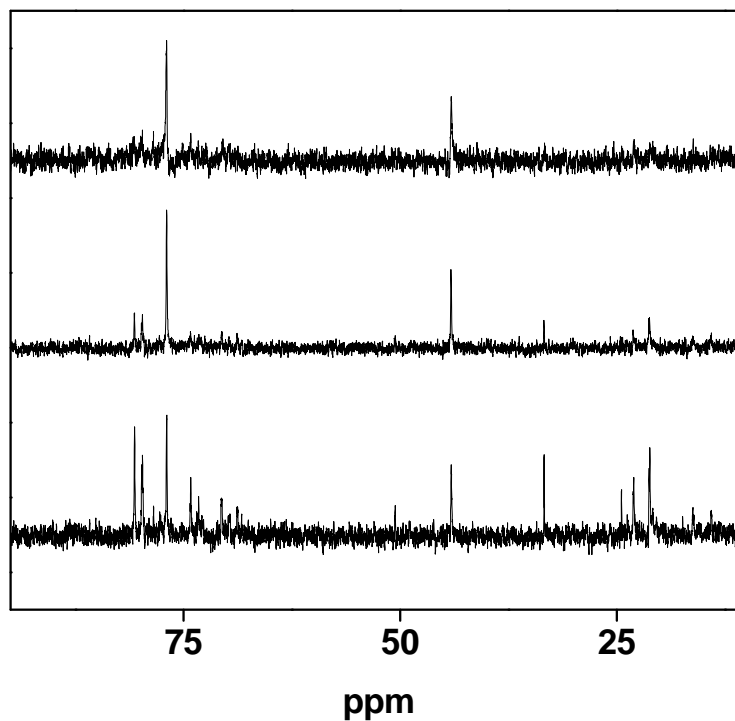


**Figure S5:** 202 MHz  $^{31}\text{P}$  NMR spectra ( $\text{CD}_2\text{Cl}_2$ ) of  $[\mathbf{2}'](\text{BARF}_{24})_2$  at  $-70\text{ }^\circ\text{C}$  (top) after warming to  $-65\text{ }^\circ\text{C}$  (middle) and  $-60\text{ }^\circ\text{C}$  (bottom).

$^{31}\text{P}$  NMR ( $\text{CD}_2\text{Cl}_2$ ,  $-70\text{ }^\circ\text{C}$ ):  $\delta$  80.7 (s, dppv), 79.8 (d, dppv), 78.5 (s, dppv), 74.1 (bs, dppv), 73.3 (s, dppv), 70.7 (s, dppv), 69.9 (bs, dppv), 68.9 (bs, dppv), 50.6 (s,  $\text{PMe}_3$ ), 33.4 (s,  $\text{PMe}_3$ ), 24.4 (s,  $\text{PMe}_3$ ), 23.8 (d,  $\text{PMe}_3$ ), 21.2 (s,  $\text{PMe}_3$ ), 20.4 (bs,  $\text{PMe}_3$ ), 16.2 (bs,  $\text{PMe}_3$ ), 14.1 (bs,  $\text{PMe}_3$ ).

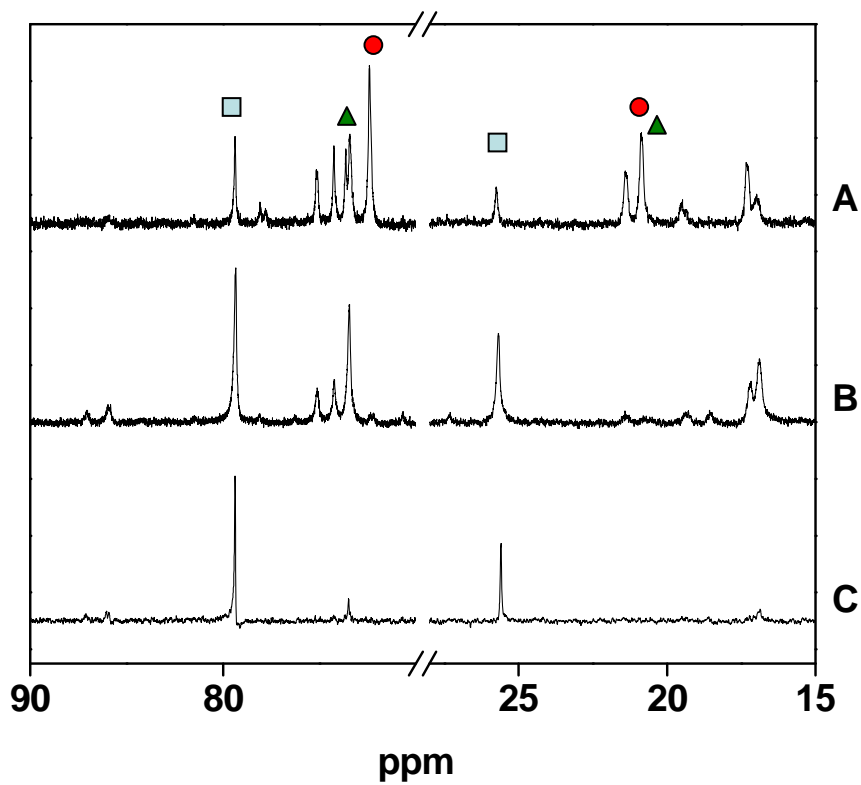


**Figure S6:** 202 MHz  $^{31}\text{P}$  NMR spectrum of  $[\mathbf{2}'](\text{BF}_4)_2$  after treatment with MeCN, and immediate room temperature work up (**A**), after  $\sim 12$  hours at  $20\text{ }^\circ\text{C}$  (**B**), and after  $\sim 48$  hours at  $20\text{ }^\circ\text{C}$  (**C**). Notice that in the initial reaction mixture, isomers A, B, and C (red circle, green triangle, and blue square, respectively) are present, but after 48 hours only isomer C remains.

#### 4. Decomposition of $[\mathbf{2}']^+$ and $[\mathbf{2}']^{2+}$ with $\text{O}_2$ .

A flask containing 0.017 g (0.020 mmol) of  $\mathbf{2}'$  and 0.032 g (0.031 mmol) of  $\text{FcBAR}_{24}^{\text{F}}$  was cooled to in a  $\text{CO}_2$ /acetone bath (a thermocouple directly inserted into the reaction mixture measure  $-71\text{ }^\circ\text{C}$ ), and to it was added 0.8 mL of  $\text{CH}_2\text{Cl}_2$ . At this point the IR spectrum indicated a mixture of  $[\mathbf{2}']^+$  and  $[\mathbf{2}']^{2+}$ . The flask was purged with 1 atm of  $\text{O}_2$  and the reaction mixture was monitored by *in site* IR spectroscopy (ReactIR 4000, Mettler Toledo). After  $[\mathbf{2}']^+$  was fully consumed and  $[\mathbf{2}']^{2+}$  consumption had slowed ( $\sim 35$  min), the resultant spectra were processed with ConCIRT. The identity of the products of decomposition was not explored.

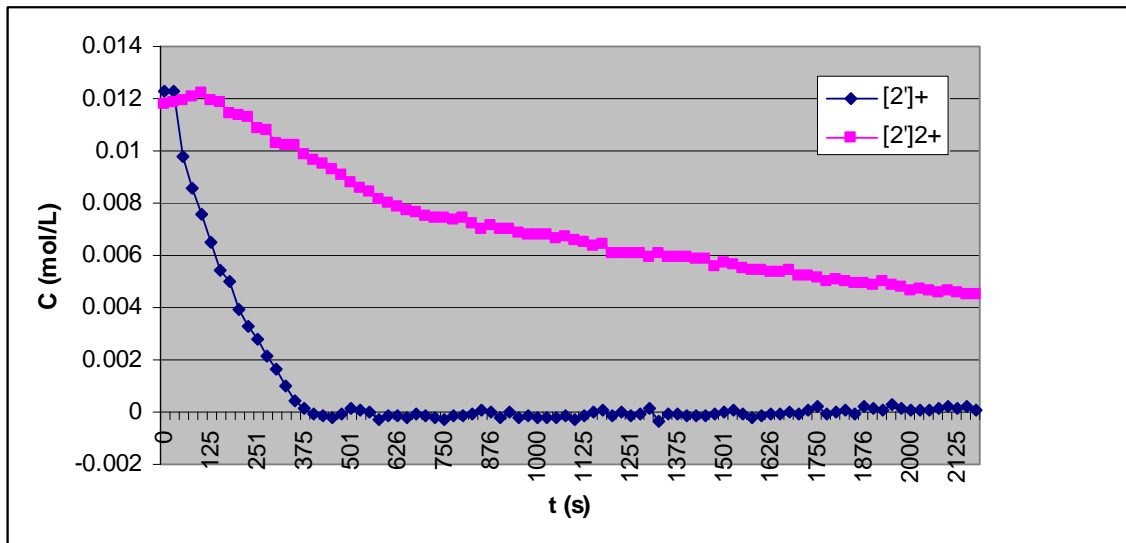
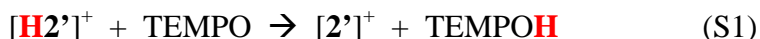


**Figure S7:** Plot of concentration vs time at  $-71\text{ }^{\circ}\text{C}$  for an equimolar mixture of  $[2']^+$  and  $[2']^{2+}$  upon treatment with 1 atm  $\text{O}_2$ . Notice that  $t_{1/2}$  for  $[2']^+$  is  $\sim 125$  s whereas  $t_{1/2}$  for  $[2']^{2+}$  is  $\sim 1200$  s.

### 5. Kinetic Analysis of the Reaction of $[\text{H}2']^+$ with TEMPO



In order to determine the rate constant of reaction S1, we performed *in situ* IR spectroscopic measurements and then simulated the resulting data.

For a typical experiment:

A mixture of 0.050 g (0.058 mmol)  $\text{Fe}_2[(\text{SCH})_2\text{NBn}](\text{CO})_3(\text{dppv})(\text{PMe}_3)$  and 0.054 g (0.058 mmol) of  $\text{H}(\text{OEt}_2)_2\text{BAr}^{\text{F}}_{24}$  were added to a flask. The flask was cooled in a cold bath of appropriate temperature, and 2.5 mL of  $\text{CH}_2\text{Cl}_2$  was added drop-wise, allowing the solvent to drip down the side of the flask. The temperature of the reaction mixture was monitored by a thermocouple that was directly inserted into the solution, and the solution was allowed to equilibrate until a steady temperature was obtained (typically  $\sim 15$  min). To the reaction mixture was added a solution of 0.009 g (0.058 mmol) TEMPO in 0.1 mL of  $\text{CH}_2\text{Cl}_2$ ; the added volume of solvent caused a temporary increase in temperature of  $\sim 3\text{ }^{\circ}\text{C}$ .

*In situ* Reaction progress was monitored by IR spectroscopy (ReactIR<sup>®</sup>, Mettler-Toledo) in the region between  $2200 - 1500\text{ cm}^{-1}$ .

Typical experimental settings consisted of a two step sequence as follows:

*Step 1.*

Duration: 2 min

Interval: Rapid Collect ( $\sim 1$  spectrum/s)

Gain: 1

Scans: 2  
Resolution: 4

*Step 2.*

Duration: 120 min  
Interval: 30 s  
Gain: 1  
Scans: 32  
Resolution: 4

Following completion of the experiment, two post-experiment processes were performed:

1. A baseline correct was performed, using the blank absorbance at 2200 cm<sup>-1</sup> for normalization.
2. Using the software application ConCIRT, the component species of the reaction profile and their relative intensities were extracted.

ConCIRT identified two major species present under these reaction conditions; the decay of [H2']<sup>+</sup> and the growth of the superimposition of [2']<sup>+</sup> and 2'. The two latter species were not distinguishable by the software under these conditions because their rate of growth was equal. Based on this observation, we propose the following reaction sequence:



The rate of S2 is much greater than S1, but can only occur to the extent that S1 occurs (i.e. TEMPOH must be generated before it can react). We independently verified that [H2']<sup>+</sup> is immediately deprotonated by TEMPOH.

Using the above model (equations S1 and S2), we simulated our data with the program Kintecus. When the reaction was performed under warmer conditions (T > 243K) or high excess concentrations of TEMPO ([TEMPO] > 0.7 M) the growth of 2' was observed to be intermittent and eventually decayed to yield a complete conversion of all Fe<sub>2</sub> species to [2']<sup>+</sup>. Under these conditions, ConCIRT was able to distinguish 2' and [2']<sup>+</sup>. The reaction scheme can be refined such that eq S2 is reversible. In this case, the equilibrium strongly favors deprotonation of [H2']<sup>+</sup> by TEMPOH, but the reverse reaction is driven by the consumption of [H2']<sup>+</sup> by TEMPO.

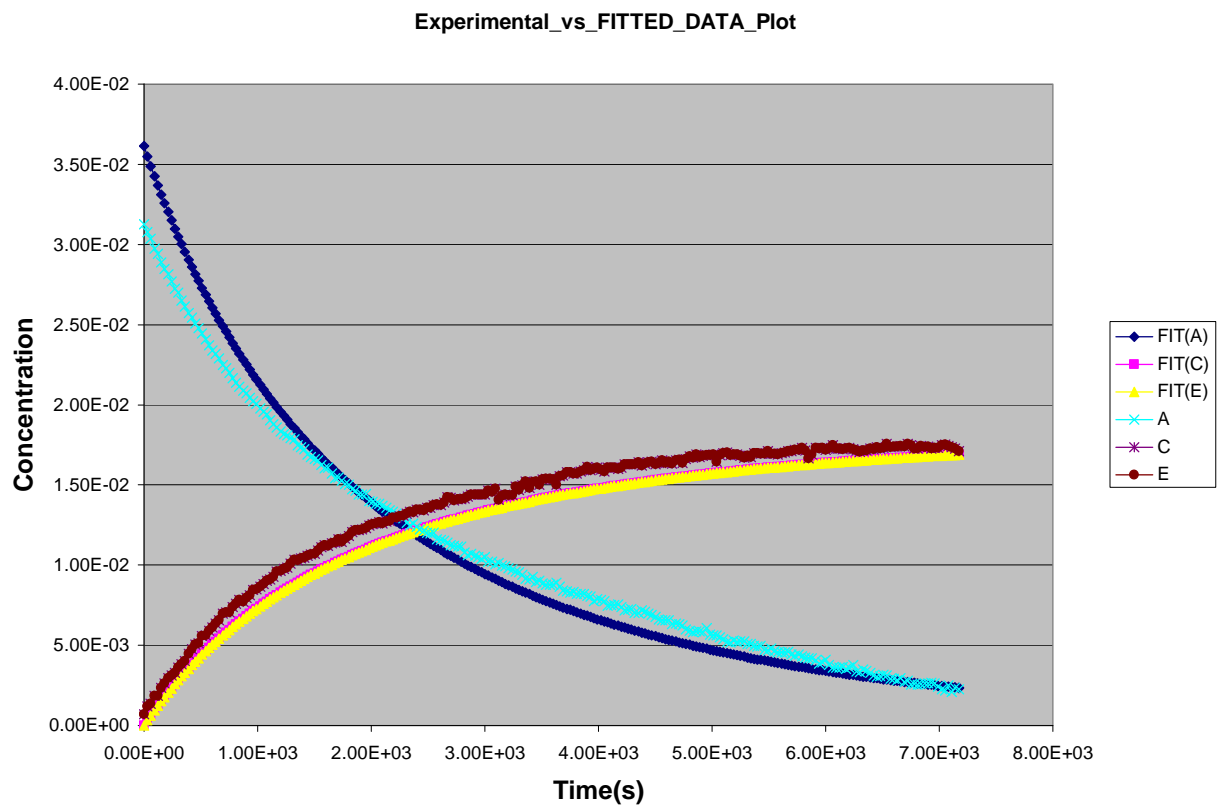


**Figure S8:** Plot of concentration vs time for experiment run at 199K. For this simulation,  $A = [H_2^{2+}]$ ,  $C = [2^{\cdot}]$ , and  $E = [2'^{+}]$ .

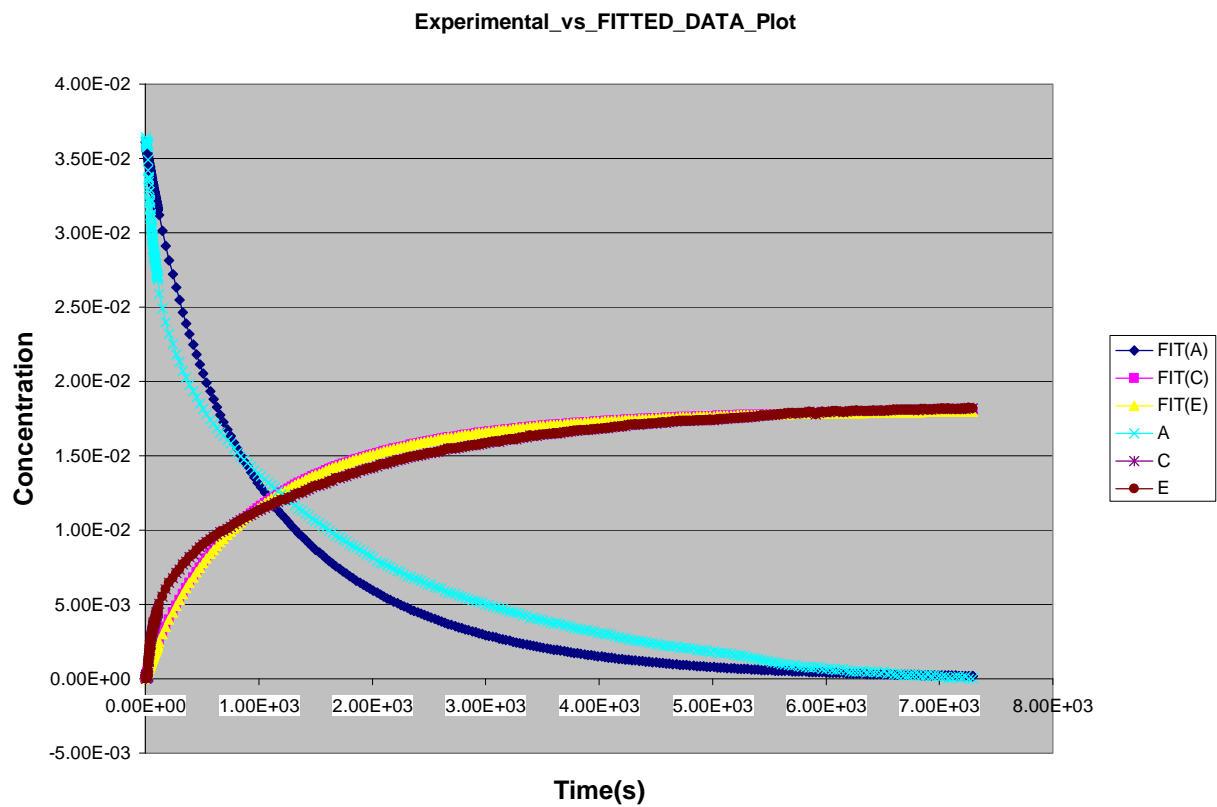


**Figure S9:** Plot of concentration vs time for experiment run at 215K. For this simulation, A =  $[H_2^{2+}]$ , C =  $[2^{\cdot}]$ , and E =  $[2^{\cdot+}]$ .

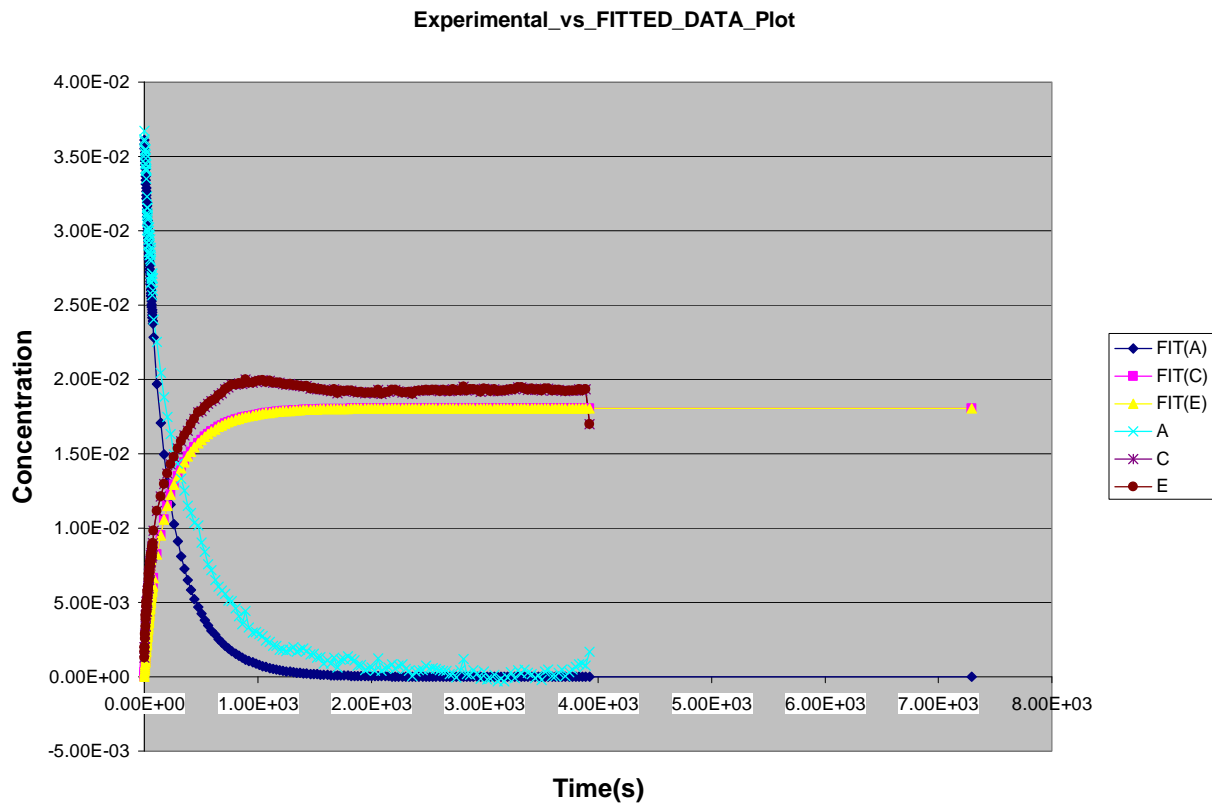


**Figure S10:** Plot of concentration vs time for experiment at 229 K. For this simulation,  $A = [H_2^{2+}]$ ,  $C = [2^{\cdot}]$ , and  $E = [2^{\cdot+}]$ . The experiment was stopped after ~4000 s, at which point it was apparent that the experiment was complete.

Figure	T	$k$
S9	229	$8.60 \times 10^{-2}$
S10	215	$1.75 \times 10^{-2}$
S11	199	$8.13 \times 10^{-3}$

**Table S1:** Rate constants ( $M^{-1}s^{-1}$ ) obtained from simulated from data sets measured at varying temperatures.

From the Eyring equation:

$$k = (k_B T/h) e^{-G^\ddagger/RT}$$

$$\ln(k/T) = -(\Delta H^\ddagger/RT) + \ln(k_b/h) + \Delta S^\ddagger/R$$

Slope of  $\ln(k/T)$  vs  $(1/T) = m = -3291.6$

$$m = -3291.6 = -\Delta H^\ddagger/R$$

$$\Delta H^\ddagger = 3291.6 \text{ K}(1.986 \text{ cal/K}\cdot\text{mol}) = 6537 \text{ cal/mol} = 6.5 \text{ kcal/mol}$$

Y-intercept of  $\ln(k/T)$  vs  $(1/T) = b = 6.2717$

$$b = 6.2717 = \ln(k_b/h) + \Delta S^\ddagger/R$$

$$\Delta S^\ddagger = (6.2717 - \ln(k_b/h))/R = (6.2717 - \ln(1.38 \times 10^{-23} \text{ cal}\cdot\text{K}^{-1} / 6.626 \times 10^{-34} \text{ J}\cdot\text{s})) \cdot 8.314 \text{ J}\cdot\text{K}^{-1}\cdot\text{mol}^{-1} = -145 \text{ J/mol}\cdot\text{K}^{-1} = -34.7 \text{ cal/mol}\cdot\text{K}^{-1} = -0.035 \text{ kcal/mol}\cdot\text{K}^{-1}$$

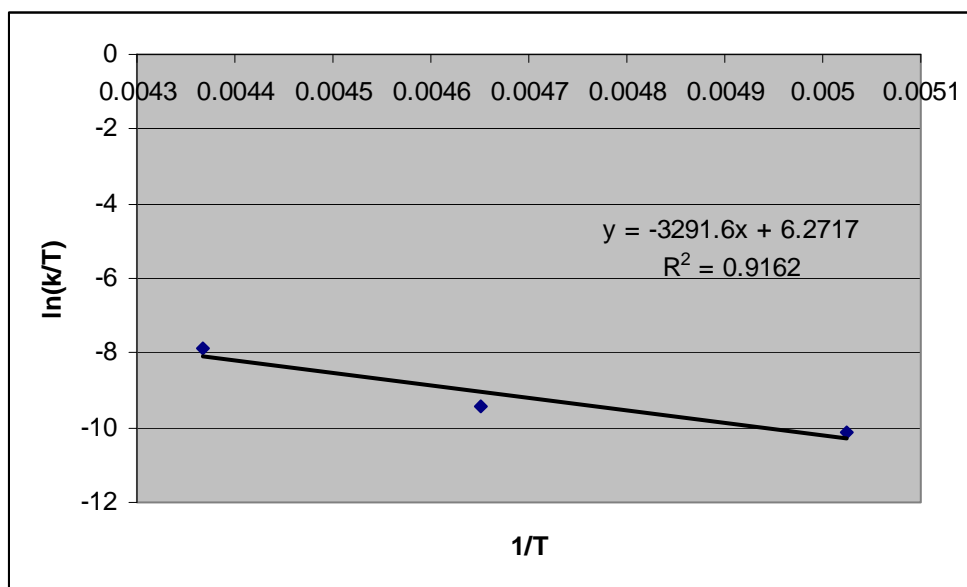


**Figure S11:** Eyring-Polanyi plot for the reaction of  $[\text{H}_2']^+$  with TEMPO at 229, 215, and 199 K.

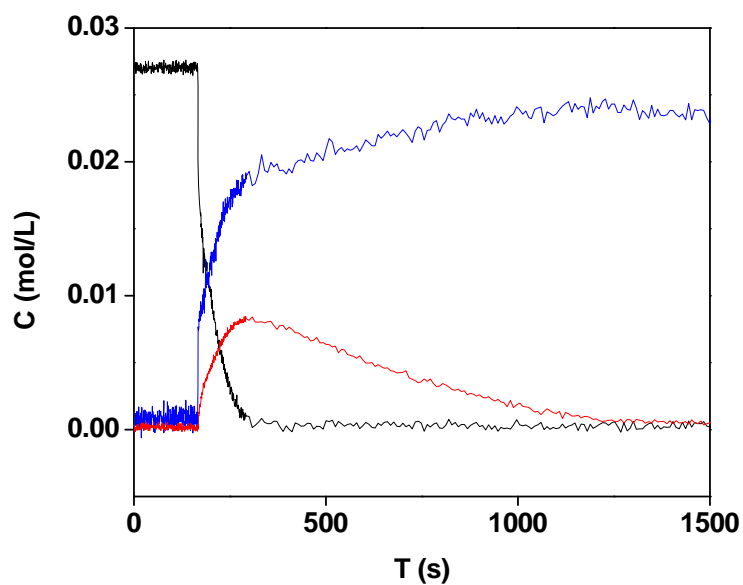


**Figure S12:** Plot of concentration vs. time for the reaction of  $[\text{H}_2']^+$  with a large excess (0.030 M  $[\text{H}_2']^+$ , 0.9 M TEMPO) of TEMPO at 210 K. Notice that the growth of  $[\text{2}']^+$  (blue) is more

rapid than the growth of **2'** (red), and that growth of **2'** stops when all of  $[\text{H2}']^+$  (black) has been consumed.

## 6. Electrochemistry

The electrochemistry of diiron dithiolates is complex and can be dramatically affected by solvent and electrolyte. The effects of donor solvents (i.e. MeCN) versus non-coordinating solvents (i.e.  $\text{CH}_2\text{Cl}_2$ ) will be discussed here.

In MeCN, **1** undergoes two reversible oxidations at -0.50 and -0.40 V. This contrasts the voltammogram observed in  $\text{CH}_2\text{Cl}_2$ , in which the second oxidation occurs at much more positive potentials. These data suggests the reversible binding of MeCN. No additional cathodic waves are observed following the oxidation events.

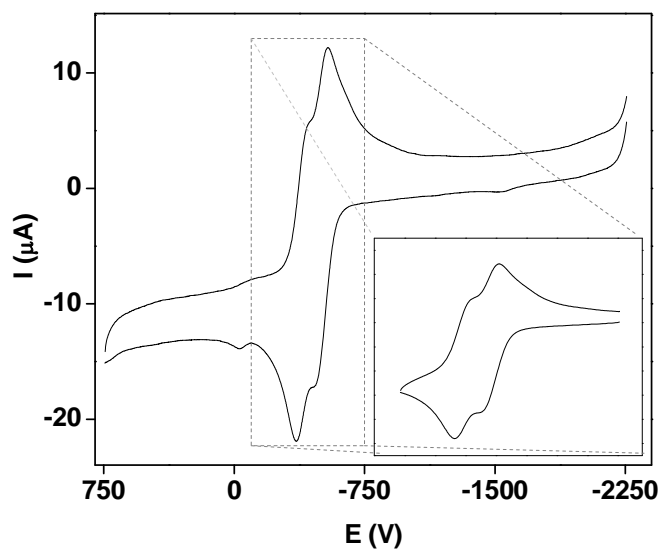


**Figure S13.** CV of **1** in MeCN solution. Conditions:  $[\text{Fe}_2] = 0.0015 \text{ M}$ ,  $[(\text{C}_4\text{H}_9)_4\text{N}]\text{PF}_6 = 0.100 \text{ M}$ , 273 K, 0.1 V/s.

**Table S2.** Potentials (V) for the  $[\text{Fe}_2(\text{SR})_2]^{0/+}$  and  $[\text{Fe}_2(\text{SR})_2]^{+/2+}$  Couples for  $\text{Fe}_2[(\text{SCH}_2)_2\text{X}](\text{CO})_3(\text{dppv})(\text{PMe}_3)$ . Conditions: 1 mM Analyte in 100 mM  $[\text{Bu}_4\text{N}]\text{PF}_6$ ;  $\text{CH}_2\text{Cl}_2$  Solution, Referenced vs  $\text{Fc}^{0/+}$ .

Dithiolate	Solvent	$E_1$ $[\text{Fe}_2(\text{SR})_2]^{0/+}$	$E_2$ $[\text{Fe}_2(\text{SR})_2]^{+/2+}$
$(\text{SCH}_2)_2\text{NBn}$ ( <b>2'</b> )	$\text{CH}_2\text{Cl}_2$	-0.643	-0.128

	MeCN	-0.565	-0.418 (estimated on half height)
(SCH <sub>2</sub> ) <sub>2</sub> CH <sub>2</sub> ( <b>1</b> )	CH <sub>2</sub> Cl <sub>2</sub>	-0.609	0.356
	MeCN	-0.504	-0.396

In MeCN, **2'** undergoes two oxidations, the first of which is reversible. On the return scan, new cathodic waves are observed at -0.8 and -0.9 V. This contrasts the voltammograms in pure CH<sub>2</sub>Cl<sub>2</sub>, there two fully reversible oxidations are observed. When CH<sub>2</sub>Cl<sub>2</sub> contain small but significant (0.08 M) amount of MeCN, the reversibility of the second oxidation is completely lost and new cathodic events are observed at 0.8 and 0.9 V.

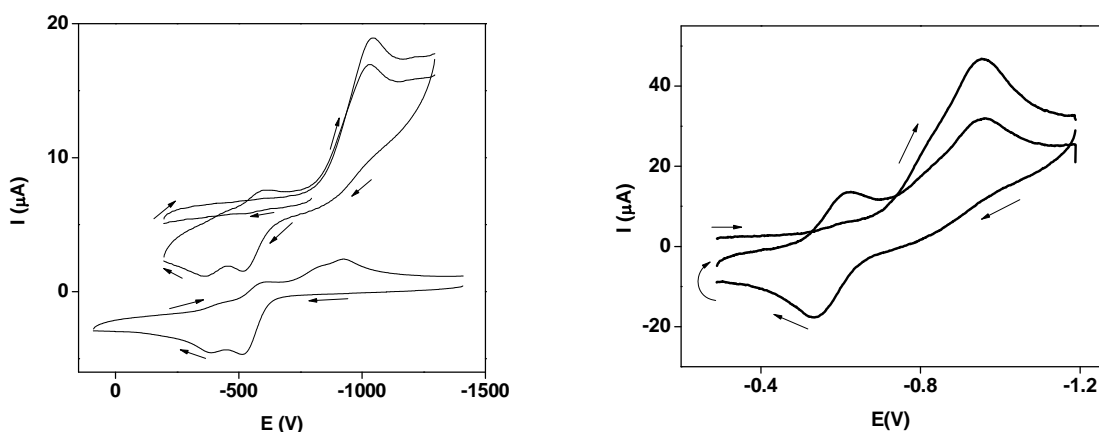


**Figure S14.** Left: Cyclic voltammogram of  $[2'(\text{MeCN})]^{2+}$  (top) and **2'** (bottom) in MeCN solution. Conditions: 0.001 M  $[\text{Fe}_2]$ , 0.100 mM  $[(\text{C}_4\text{H}_9)_4\text{N}]\text{BAR}^{\text{F}}_{24}$ ,  $\text{CH}_2\text{Cl}_2$ , 20 °C, 0.1 V/s scan rate, referenced to  $\text{Fc}^{0/+}$ . Notice that upon reduction of  $[2'(\text{MeCN})]^{2+}$ , **2'** is observed on the return scan. Additionally, notice that upon oxidation of **2'**,  $[2'(\text{MeCN})]^{2+}$  is observed on the return scan.

Right: Cyclic voltammogram of  $[2'(\text{MeCN})]^{2+}$  in  $\text{CH}_2\text{Cl}_2$  solution. Conditions: 0.001 M  $[\text{Fe}_2]$ , 0.300 mM  $[(\text{C}_4\text{H}_9)_4\text{N}]\text{BAR}^{\text{F}}_{24}$ ,  $\text{CH}_2\text{Cl}_2$ , 20 °C, 0.5 V/s scan rate, referenced to  $\text{Fc}^{0/+}$ . Notice that the electrochemical properties of  $[2'(\text{MeCN})]^{2+}$  are similar in  $\text{CH}_2\text{Cl}_2$ , however the first oxidation event is now reversible.

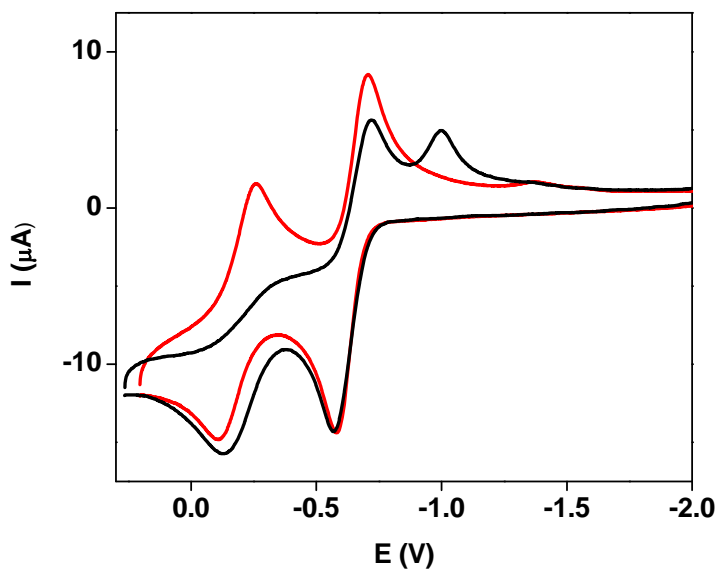


**Figure S15.** Cyclic voltammograms of a  $\text{CH}_2\text{Cl}_2$  solution of  $2'$  in pure  $\text{CH}_2\text{Cl}_2$  (red) and in  $\text{CH}_2\text{Cl}_2$  containing 0.08 M MeCN (black). Notice that upon addition of MeCN,  $E_2$  becomes fully irreversible and a cathodic wave is observed at -0.9 V. Conditions: 0.001 M  $2'$ , 0.300 M  $[(\text{C}_4\text{H}_9)_4\text{N}]\text{PF}_6$ ,  $\text{CH}_2\text{Cl}_2$ , 20 °C, 0.1 V/s scan rate.

The bridging hydride  $[2'(\mu\text{-H})]^+$  displays a quasi-reversible reduction that is fully irreversible below 0.050 V/s, but gains reversibility at faster scan rates.

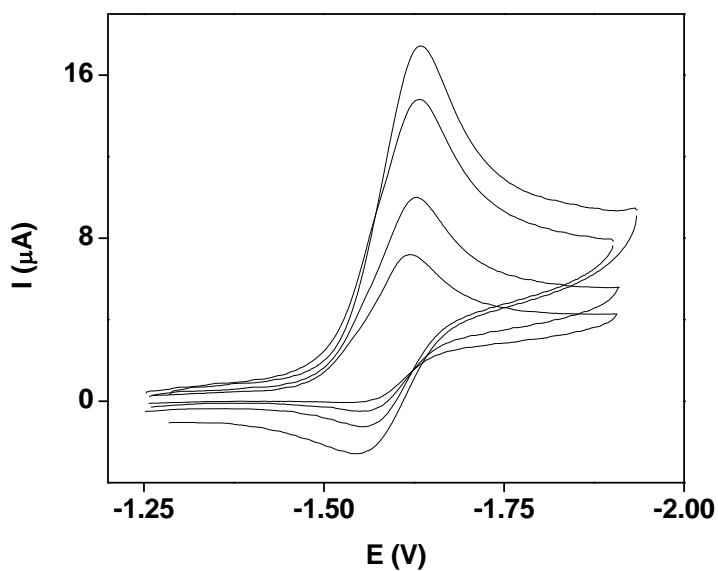


**Figure S16.** CV of  $[2'(\mu\text{-H})]^+$  in MeCN solution at 0.025, 0.050, 0.100, and 0.200 V/s.  
Conditions:  $[\text{Fe}_2] = 0.0015 \text{ M}$ ,  $[(\text{C}_4\text{H}_9)_4\text{N}]\text{PF}_6 = 0.100 \text{ M}$ , 273 K.

1. Rackowski Dubois, M.; Dubois, D. L., *Chem. Soc. Rev.*, **2009**, 38, 62-72.
2. Wayner, D. A.; Parker, V. D., *Acc. Chem. Res.*, **1993**, 26, 287-294.
3. Stanley, J. L.; Heiden, Z. M.; Rauchfuss, T. B.; Wilson, S. R.; De Gioia, L.; Zampella, G., *Organomet.*, **2008**, 27.
4. Olsen, M. T.; Barton, B. E.; Rauchfuss, T. B., *Inorg. Chem.*, **2009**, 48, 7507-7509.
5. Bruschi, M.; Fantucci, P.; De Gioia, L., *Inorg. Chem.*, **2004**, 43, 3733-3741.